J Mater Sci (2011) 46:4085–4091
DOI 10.1007/s10853-011-5410-2

LETTER

Two-stage crystallization kinetics equation and nonisothermal crystallization analyses for PTEG and filled PTEG

Yong Xu · Songmin Shang · Jian Huang · Sinchi Wan

Published online: 3 March 2011

Abstract A novel modified Avrami model considering both primary and secondary crystallization has been presented to extract the kinetic behavior of these two crystallization stages in nonisothermal crystallization process of polymers. Nonisothermal crystallization kinetics of poly(trimethylene terephthalate)–poly(ethylene glycol) segmented copolyesters (PTEG) has been investigated by differential scanning calorimetry. The crystallization rate constants and Avrami exponents at various cooling rates were obtained from the analyses for neat PTEG and multiwalled carbon nanotube (MWNT) filled PTEG. Secondary crystallization displays a lower-dimensional crystal growth compared with primary crystallization and the results of kinetics analyses are consistent with morphology study. The MWNTs introduced into PTEG matrix take the role of effective nucleating agents during composites crystallization and can expedite the process of crystallization of the matrix by providing more nucleation sites to the crystallizing phase.

Y. Xu (✉)
Department of Polymer Science and Engineering,
Nanjing University of Science and Technology,
Nanjing 210094, China
e-mail: xuyong@zuaa.zju.edu.cn

S. Shang · S. Wan
Institute of Textiles and Clothing,
The Hong Kong Polytechnic University,
Hong Kong, China

J. Huang
Department of Chemistry,
University of Texas at San Antonio,
San Antonio, TX 78249-1644, USA

The subject of crystallization kinetics for polymers has been of great interest for several decades and still provides fruitful areas for research [1]. Crystallization process of polymers can be studied under either isothermal condition or nonisothermal condition. Isothermal experiments are generally carried out [1, 2] because the theoretical analysis is easy to handle and problems associated with cooling rates and thermal gradients within specimens can be avoided. In practice, however, from a scientific point of view, the study of crystallization in nonisothermal conditions may expand our general understanding of the crystallization behavior of polymers since many isothermal methods are often restricted to narrow temperature ranges and industrial processes normally proceed under nonisothermal conditions. Therefore, more and more attention has been paid to the nonisothermal crystallization process of polymers.

Analysis of the overall crystallization rate under isothermal conditions is commonly accomplished with the use of the Avrami equation that permits one to calculate the crystallinity fraction, X_t, as a function of the elapsed time [3–5]:

$$X_t = 1 - \exp(-Kt^n) \tag{1}$$

where K is the crystallization rate constant and n is the Avrami exponent which contains information on nucleation and growth geometry. To study the kinetic parameters for nonisothermal crystallization processes, several models have been developed. The majority of the proposed formulations are based on the Avrami theory, such as Jeziorny equation [6], Ozawa equation [7], and Ziabicki equation [8]. A novel method developed by Mo was also employed by combining the Avrami and Ozawa equations [9].

Among the theories reported, Ozawa equation has been most successfully applied to the analysis of dynamic solidification:

$$X_t = 1 - \exp\left(\frac{-K^*}{\phi^m}\right) \quad (2)$$

where ϕ is the cooling rate, m is the Ozawa exponent, and K^* is the Ozawa cooling crystallization function. Nonisothermal crystallization data for many polymers can be fitted by the Ozawa equation [1].

However, for polymers like poly(ether ether ketone) (PEEK), polyethylene (PE), nylon 11, copolyesters [9–12], etc., their dynamic solidification kinetics were not described adequately by the Ozawa method. The study of the nonisothermal crystallization of a phase-separated poly(epsilon-caprolactone)/poly(ethylene oxide) (PCL/PEO) diblock copolymer has been performed by Gan et al. [11]. They found that the experimental data showed no agreement with the Ozawa model which probably because the secondary crystallization (SC) could not be neglected. The analysis of nonisothermal crystallization of PEEK with the Ozawa treatment was also failed [12]. The reason for the curvature in the plots was attributed to SC processes which, for PEEK, contribute from 45 to 70% of the total crystallinity developed. Curvature in Ozawa plots became evident when the X_t values at the chosen temperature included values selected from the primary crystallization (PC) rate at one rate and the SC process at another rate. For example, at 563 K the initial portion of the 20 K/min curve overlapped the primary portion of the 10 K/min and the secondary portion of the 5 and 2 K/min curves. The Ozawa analysis failed to describe the dynamic solidification of poly(ether ether ketone ketone) (PEEKK) [9]. The nonisothermal crystallization behavior of ethylene terephthalate–ethylene oxide segmented copolyesters has been studied by Kong et al. [10], the experimental data reported were also not sufficient to allow a proper description of dynamic solidification kinetics with the Ozawa approach.

The study of nonisothermal crystallization kinetics for the crystalline polymers whose SC process contributes the important proportion of the total crystallinity in their crystallization windows, is of importance for their process modeling and crystallization control. However, to our knowledge, few kinetics models for nonisothermal crystallization have been presented to deal with the secondary crystallization process so far.

In this letter, an attempt has been made to find the parameters of the Avrami equation applied to nonisothermal crystallization for both the primary and the secondary crystallization processes. The experiments were performed for poly(trimethylene terephthalate)–poly(ethylene glycol) segmented copolyesters (PTEG). For the purpose of comparison, PTEG filled with multi-walled carbon nanotubes (MWNTs) were prepared by solution blending and their crystallization kinetics was also evaluated.

Poly(trimethylene terephthalate) (PTT) is a typical semicrystalline polymer and recently attracted much attention owing to its outstanding characteristics, such as superior elastic recovery, good colorfastness, uniform dye uptake, stain resistance, since its development for fibers and engineering thermoplastics [13–15]. To achieve novel linear thermoplastic copolyesters with modified crystallization properties, PTT was copolymerized using several amounts of the second glycol or diacid comonomer [16, 17] and PTEG was also presented in which PTT was used as the rigid segment in the multiblock copoly(ether-ester)s, while polyethylene glycol (PEG) was used as the flexible segment [18]. However, to our knowledge, no nonisothermal crystallization kinetics for PTEG has been reported in spite of its potential academic and technological values.

PTEG used in this study is the same polymer which has been described in one of our previous articles [18]. The molecular characteristics are listed in Table 1 and the chemical structure has been determined by C^{13} nuclear magnetic resonance spectrum using a Bruker AM 500 as shown in Fig. 1 (molecular characteristics and the chemical structure are abstracted from Ref. [18]). In this study, the PEG used to be polymerized into PTT is PEG2000, i.e., it has a number-average molecular weight of about 2000, and has 11.24 wt% in the resultant PTEG. MWNTs, serve as nucleating fillers [19], were purchased from Bill Nanotech

Table 1 Compositions, intrinsic viscosities, number-average molecular weights, and melting point of PTEG used

Composition in mol ratio[a] (1,3PDO/PEG/TPA)	Mass fraction of PEG in copolyester	$[\eta]$[b] (m^3/kg)	$\overline{M_n}$[c]	$T_m^{d,e}$ (K)
0.98602/0.01526/1	11.24	0.0835	59480	497.2

1,3PDO 1,3-propanediol, *TPA* terephthalic acid

[a] Measured by ^{13}C NMR spectroscopy

[b] Measured in the solution of 1:1 (w/w) 1,1,2,2-tetrachloroethane/phenol at 298 K

[c] Estimated from the measured intrinsic viscosities

[d] Measured by DSC at a scanning rate of 10 K/min

[e] Melting point

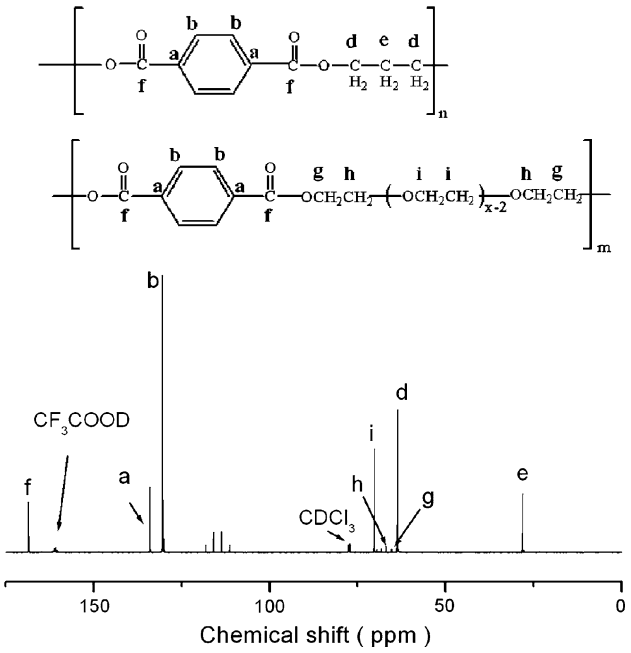

Fig. 1 ^{13}C-NMR spectrum and chemical shifts assignment of PTEG

Co., Ltd (Shenzhen, China). These MWNTs were produced via the chemical vapor deposition (CVD) method and have lengths up to a few microns and diameters between 70 and 100 nm. The purchased MWNTs were purified by aqueous HNO_3 to remove amorphous carbon and iron impurities and then functionalized by tetrabutyl titanate to enhance the compatibility of MWNTs with PTEG. To fabricate PTEG/MWNT composites, weighed PTEG sample was dissolved in the solution of 1:1 (w/w) 1,1,2,2-tetrachloroethane/phenol at 353 K to form a clear solution. Appropriate amount of functionalized MWNTs was weighed according to the required percentage and added into the solution. The mixture was refluxed with stir for 4 h to form a homogeneous suspension and then sonicated for 1 h. Finally, the mixture was cast into an aluminum mold in the form of a film and then dried by vacuum at 373 K for 48 h. The final nanocomposite is the copolyester filled with MWNTs which have a weight percent of 0.1% in the composite (denoted as PTEG–MWNT 99.9/0.1).

Differential scanning calorimetry (DSC) measurements were carried out on a TA Q200 equipment, calibrated with indium and tin standards, under a nitrogen atmosphere. The specimens were heated to 533 K at a scanning rate of 10 K/min, and kept at this temperature for 5 min in order to remove the thermal history. The DSC cooling traces were recorded at the rates of 2, 5, 10, and 30 K/min, respectively. For an accurate determination of the nonisothermal kinetic characteristics, the apparatus was calibrated at various scanning rates. Samples for polarized optical microscopy (POM) observation were prepared by sandwiching a tiny particle of PTEG or the corresponding nanocomposite between two glass plates and compressing at 533 K for 3 min and then quenching to room temperature. POM observation was performed using an Olympus BX50 hot-stage microscope which equipped with a liquid N_2 cooling and temperature control system. The nonisothermal crystallization was carried out like that of DSC by first heating the sample to 533 K and maintaining this temperature for 5 min, and then cooling to room temperature at a rate of 5 K/min. The PTEG sample after DSC measurement was carefully taken out from the measuring cell and observed using a FEI SIRION scanning electron microscope (SEM).

Under nonisothermal conditions, the Avrami equation can be rewritten simply as:

$$X_t = \frac{\int_0^t \left(\frac{dH}{dt}\right)dt}{\int_0^\infty \left(\frac{dH}{dt}\right)dt} = 1 - \exp(-Zt^n) \tag{3}$$

where dH/dt is the heat flow rate of a DSC exotherm, X_t can be obtained from the area of the DSC exothermic peak at the time t divided by the total area under the exothermic peak, n is the Avrami exponent, Z is the crystallization rate constant. For the nonisothermal crystallization process, Z does not have the same physical meaning as in the isothermal crystallization process since the temperature changes instantly. Assuming a constant ϕ (the cooling rate of the nonisothermal crystallization), the form of the parameter characterizing the kinetics of nonisothermal crystallization was corrected to [6]:

$$\log(Z_c) = \frac{\log(Z)}{\phi} \tag{4}$$

The values of the Avrami exponent n and the rate constant Z can be determined from the slope and the intercept of the plot of $\log[-\ln(1 - X_t)]$ versus $\log t$. As in the isothermal studies by Velisaris et al. [20] and Verhoyen et al. [5], we supposed that the SC process in nonisothermal crystallization is also an Avrami process. Since its kinetics differ greatly from those of the primary one, another essential assumption is that the two processes have independent heat releases. Thus the time dependence of crystallinity in the PC process and SC process is given, respectively:

$$X_{p,t} = \frac{\int_0^t \left(\frac{dH}{dt}\right)dt}{\int_0^{t_{p,end}} \left(\frac{dH}{dt}\right)dt} = 1 - \exp\left(-Z_p t^{n_p}\right) \tag{5}$$

$$X_{s,t} = \frac{\int_{t_{p,end}}^{t-t_{p,end}} \left(\frac{dH}{dt}\right)dt}{\int_{t_{p,end}}^\infty \left(\frac{dH}{dt}\right)dt} = 1 - \exp\left(-Z_s\left(t - t_{p,end}\right)^{n_s}\right) \tag{6}$$

where $t_{p,end}$ is the time at which the primary process finishes and the secondary one starts. Z_p, n_p and Z_s, n_s are Avrami constants in the two consecutive processes,

respectively. $X_{p,end}$ the crystallinity at the end of the primary process, and X_s the total crystallinity developed in the secondary one can be expressed as:

$$X_{p,end} = \frac{\int_0^{t_{p,end}} \left(\frac{dH}{dt}\right) dt}{\int_0^{\infty} \left(\frac{dH}{dt}\right) dt} \quad (7)$$

$$X_s = \frac{\int_{t_{p,end}}^{t-t_{p,end}} \left(\frac{dH}{dt}\right) dt}{\int_0^{\infty} \left(\frac{dH}{dt}\right) dt} \quad (8)$$

Thus, Eqs. 5 and 6 are reduced to

$$X_{p,t} = \frac{X_t}{X_{p,end}} = 1 - \exp\left(-Z_p t^{n_p}\right) \text{ (PC process)} \quad (9)$$

$$X_{s,t} = \frac{X_t - X_{p,end}}{X_s} = 1 - \exp\left(-Z_s \left(t - t_{p,end}\right)^{n_s}\right) \text{ (SC process)} \quad (10)$$

Meanwhile,

$$\log\left(Z_{c,p}\right) = \frac{\log\left(Z_p\right)}{\phi} \quad (11)$$

$$\log\left(Z_{c,s}\right) = \frac{\log\left(Z_s\right)}{\phi} \quad (12)$$

when $X_{p,end} = 1$, Eq. 10 is equivalent to Eqs. 3 and 10 as well as Eq. 12 has no relevance because the secondary process would not take place. Utilizing this model, one can obtain the Avrami kinetic parameters of the PC and SC processes of polymers from nonisothermal crystallinity data, the relationship between crystallization t and crystallization temperature T is given by:

$$t = \frac{T_0 - T}{\phi} \quad (13)$$

where T is the temperature at time t, T_0 is the initial temperature when crystallization begins ($t = 0$).

Typical plots of the dynamic crystallization are shown in Fig. 2. It is seen that the crystallization exotherm shifts to lower temperatures with increasing cooling rates for both neat PTEG and PTEG-MWNT 99.9/0.1, respectively. Figure 3 showed the developments of the relative crystallinity as a function of crystallization time t at different cooling rates. The plot of $\log(-\ln(1 - X_t))$ versus $\log t$ (from Eq. 3) did not yield a single straight line, as shown in Fig. 4. In fact, each curve has an inflection and this deviation is usually considered to be due to the SC process, which is caused by the spherulite impingement in the later stage [14]. For distinguishing and analyzing the primary and the secondary processes, it is very important to determine a critical crystallinity, $X_{p,end}$, which marks the completion of the primary crystallization. In this work, $X_{p,end}$ was obtained from a critical value of $L_{p,end}$ ($L_{p,end} = \log[-\ln(1 - X_{t,end})]$). Figure 5 gives an example to help understanding how to determine $L_{p,end}$.

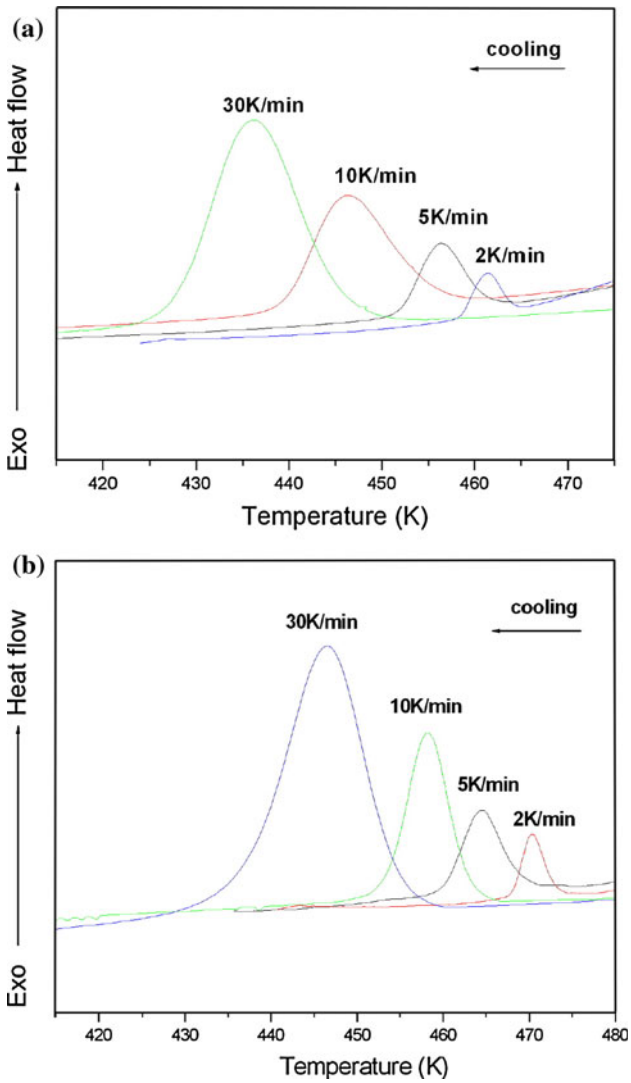

Fig. 2 DSC scans of **a** neat PTEG and **b** PTEG-MWNT 99.9/0.1 nonisothermal crystallization at different cooling rates

Near the demarcation point ($X_{p,end}$) of the PC process and the SC process, the second part in the plot sometimes bends slightly. In this case, the data near the demarcation point will be ignored and the main data which compose the straight line will be considered to calculate the slope. Analysis of the curves obtained according to Eqs. 9 and 10 (assuming a two-stage crystallization process) gives the data in Table 2. The growth rate constants in PC process, $Z_{c,p}$s, both for neat PTEG and PTEG-MWNT 99.9/0.1 increased with increasing cooling rate. That is reasonable since Z_c is a measure of the crystallization rate, which gets faster with supercooling. A strong dependence of these constants on the rate of cooling can be seen. Within the range of cooling rates 2–30 K/min, the rate constant of crystallization of PTEG in the PC process increases approximately 128×, and that ($Z_{c,s}$) of the SC process

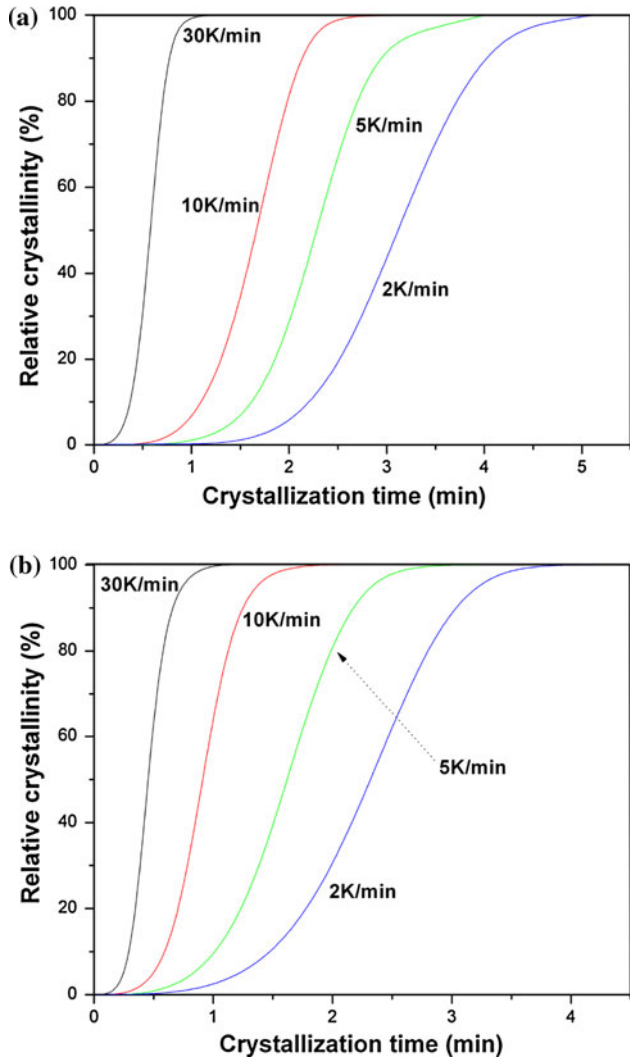

Fig. 3 Development of relative crystallinity for **a** neat PTEG and **b** PTEG-MWNT 99.9/0.1 as a function of time in nonisothermal crystallization

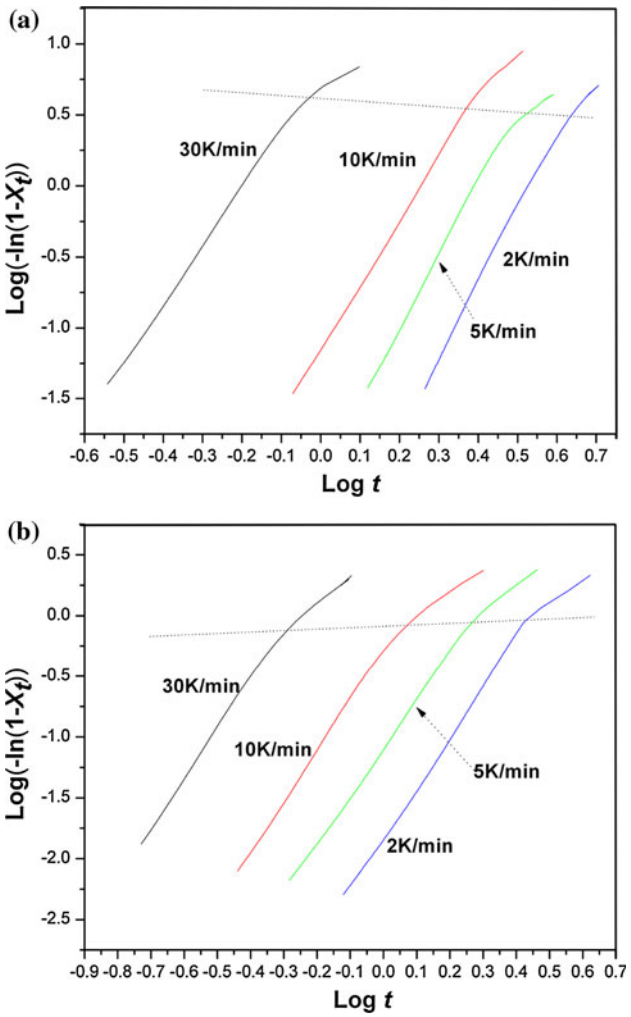

Fig. 4 Avrami curves for **a** neat PTEG and **b** PTEG-MWNT 99.9/0.1 in nonisothermal crystallization

increases 49×. For PTEG-MWNT 99.9/0.1, these two parameters increase 95× and 50×, respectively. Furthermore, the values of $Z_{c,p}$s and $Z_{c,s}$s of PTEG-MWNT 99.9/0.1 are always larger than those of neat PTEG for a fixed cooling rate. This proves that the crystallization has been accelerated because of the presence of the nanoparticles for both PC and SC process.

Although the fractional values of Avarmi exponent listed in Table 2 make the proposition of the well-defined mechanism of crystallization somewhat difficult, it can be used to qualitatively signify the mechanism of crystallization [21]. The value of about 3.3–3.6 of n_p for neat PTEG indicates a threedimensional spherulite growth and is still indicative of heterogeneity in the process because the theoretical value of Avrami exponent should be 4.0 for threedimensional growth with homogeneous nucleation. This may be attributed to

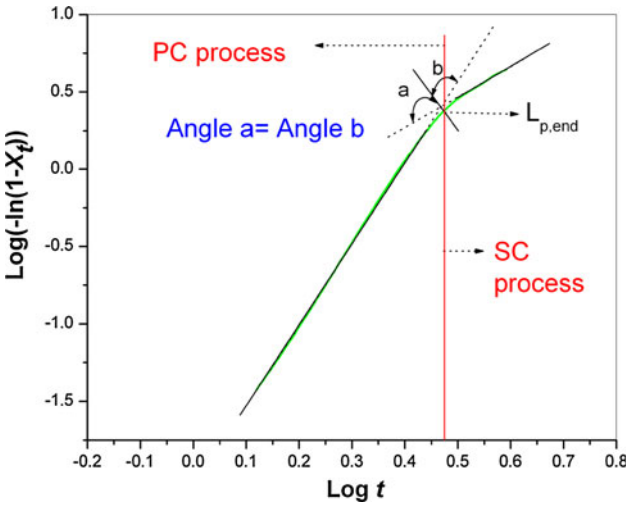

Fig. 5 Determination of $L_{p,end}$ for neat PTEG at a cooling rate of 5 K/min

Table 2 Nonisothermal crystallization kinetic parameters for PTEG and PTEG-MWNT 99.9/0.1 based on two-stage Avrami analysis

Sample	ϕ (K/min)	n_p	$Z_{c,p}$ (min^{-n})	n_s	$Z_{c,s}$ (min^{-n})
PTEG	2	3.5	0.023	1.3	0.012
	5	3.4	0.077	1.2	0.042
	10	3.6	0.215	0.9	0.176
	30	3.3	2.950	1.2	1.136
PTEG-MWNT99.9/0.1	2	2.7	0.217	1.4	0.145
	5	3.0	0.548	0.7	0.359
	10	2.9	1.039	1.1	0.977
	30	2.6	9.322	1.3	7.303

the presence of polymerization catalyst in the resultant PTEG which can act as the heterogeneous nucleating agent in the crystallization process. In particular, the decreased n_p values (ranged from 2.7 to 3.0) for PTEG-MWNT 99.9/0.1 samples are probably due to the presence of MWNTs induced more heterogeneous nucleation.

The n_s values of the SC process for both neat PTEG and PTEG-MWNT 99.9/0.1 were limited from 0.7 to 1.4, suggesting that the growth mechanisms are the same in the cooling rate range investigated. The exact mechanism of the polymer secondary crystallization has still been in dispute [22, 23]. According to the Avrami theory, the changing of Avrami exponent from about 3 to about 1 indicates that the crystallization mode might shift to one-dimensional crystal growth caused probably by spherulite impingement [21]. Figure 6 gives the crystallization morphologies of dynamic crystallized PTEG and PTEG-MWNT 99.9/0.1. For the neat PTEG crystallized at cooling rates of both 2 and 10 K/min, spherulites are fairly big and perfectly grown with maltese crosses, and have clear boundaries formed in the SC process. Compared with the neat PTEG, PTEG-MWNT 99.9/0.1 shows the formation of very tiny spherulites in the same condition and the microstructures cannot be accurately discovered. This may be because the nucleation density of PTEG matrix is greatly increased and the spherulites size is apparently decreased in the nanocomposite. To further illustrate the impingement of spherulites caused by secondary crystallization, the surface and cross-section of the PTEG sample obtained, after the DSC study, were observed by FE-SEM as shown in Fig. 7. After the nonisothermal crystallization,

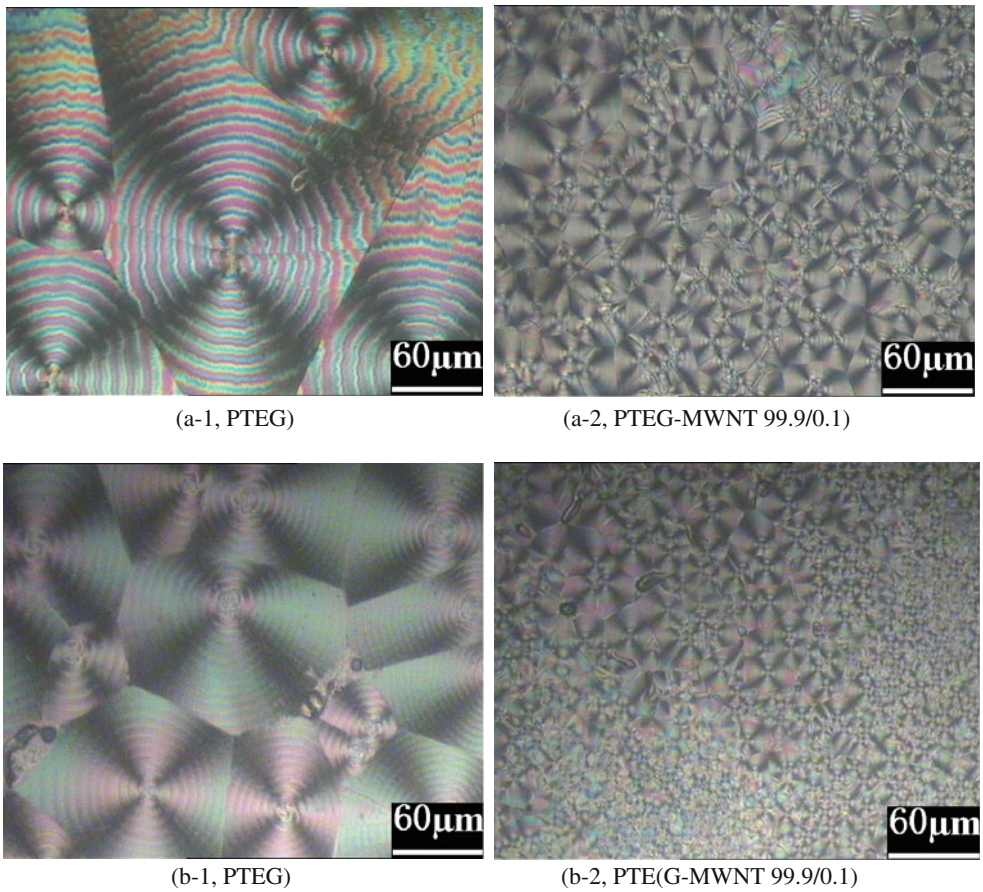

(a-1, PTEG) (a-2, PTEG-MWNT 99.9/0.1)

(b-1, PTEG) (b-2, PTE(G-MWNT 99.9/0.1)

Fig. 6 Crystallization morphology of PTEG and PTEG-MWNT 99.9/0.1 at cooling rates of **a** 2 K/min, **b** 10 K/min

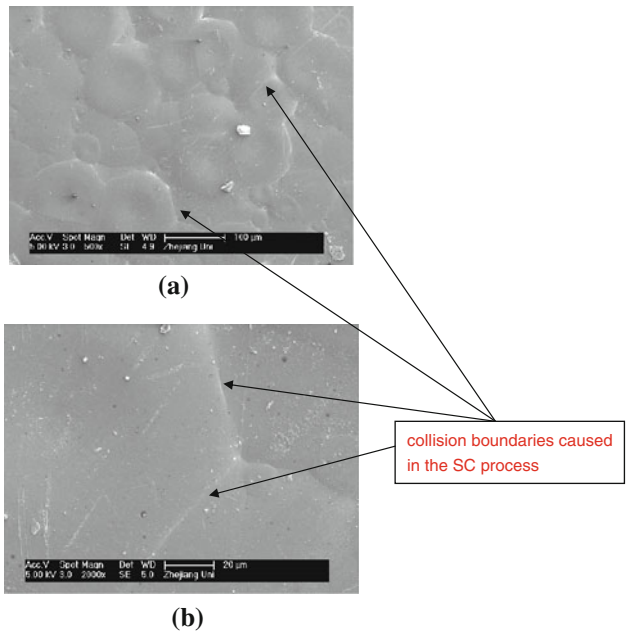

Fig. 7 SEM images of PTEG crystallized at a cooling rate 2 K/min: **a** the surface **b** higher magnification image of part of **a**

the spherulites impinged on one another with more or less boundaries and especially, on the surface of the sample, straight dividing lines of spherulites had formed. Detailed studies of nonisothermal crystallization behavior including the secondary crystallization process for PTEG with emphasis on the relationship between the soft hard segment structure and the crystallization kinetics are in progress and will be published shortly.

Acknowledgements The work was supported by a grant of The Hong Kong Polytechnic University (934K) and a grant from The Doctoral Fund of Ministry of Education of China (No. 200802881030).

References

1. Lorenzo MLD, Silvestre C (1999) Prog Polym Sci 24:917
2. Piorkowska E, Galeski A, Haudin JM (2006) Prog Polym Sci 31:549
3. Avrami M (1941) J Chem Phys 9:177
4. Mandelkern L, Quinn FA, Flory PI (1954) J Appl Phys 25:830
5. Verhoyen O, Dupret F, Legras R (1998) Polym Eng Sci 38:1594
6. Jeziorny (1978) Polymer 19:1142
7. Ozawa T (1971) Polymer 12:150
8. Ziabicki A, Sajkiewicz A (1998) Colloid Polym Sci 276:680
9. Liu T, Mo Z, Wang S, Zhang H (1997) Polym Eng Sci 37:568
10. Kong XH, Yang XN, Zhou E, Ma D (2000) Eur Polym J 36:1085
11. Gan Z, Zhang J, Jiang B (1997) J Appl Polym Sci 63:1763
12. Cebe P, Hong SD (1986) Polymer 27:1183
13. Yao C, Yang G (2010) Polymer 51:1516
14. Heschmeyer C (2000) Int Fiber J 4:66
15. Xu Y, Ye SR, Bian J, Qian JW (2004) J Mater Sci 39:5551. doi:10.1023/B:JMSC.0000039285.56017.c6
16. Xu Y, Ye SR, Bian J, Qian JW (2005) J Mater Sci 40:2039. doi:10.1007/s10853-005-1228-0
17. Jia HB, Xu Y, Ye SR, Bian J, Qian JW (2006) J Mater Sci 41:4970. doi:10.1007/s10853-006-0136-2
18. Xu Y, Jia HB, Ye SR, Huang J (2007) J Mater Sci 42:8381. doi:10.1007/s10853-007-1937-7
19. Bhattacharyya AR, Sreekumar TV, Tao L, Kumar S, Ericson LM, Hauge RH, Smalley RE (2003) Polymer 44:2373
20. Velisaris CN, Seferis JC (1986) Polym Eng Sci 26:1574
21. Wunderlich B (1976) Macromolecular physics, vol 2. Academic Press, New York
22. Wang ZG, Hsia BS, Sauer BB, Kampert WG (1999) Polymer 40:4615
23. Zachmnn HG (1995) Nucl Instrum Methods Phys Res B 97:209